Mon. Not. R. Astron. Soc. **398,** 1505–1511 (2009) doi:10.1111/j.1365-2966.2009.15208.x

On the incidence of magnetic fields in slowly pulsating B, β Cephei and B-type emission-line stars

J. Silvester,[1,2⋆] C. Neiner,[3] H. F. Henrichs,[4] G. A. Wade,[2] V. Petit,[5] E. Alecian,[2] A.-L. Huat,[6] C. Martayan,[6,7] J. Power[2] and O. Thizy[8]

[1]*Department of Physics, Engineering Physics & Astronomy, Queen's University, Kingston, Ontario, Canada K7L 3N6*
[2]*Department of Physics, Royal Military College of Canada, PO Box 17000, Station 'Forces', Kingston, Ontario, Canada K7K 7B4*
[3]*GEPI, Observatoire de Paris, CNRS, place Jules Janssen, 92190 Meudon Cedex, France*
[4]*Astronomical Institute 'Anton Pannekoek', University of Amsterdam, Science Park 904, 1098 XH Amsterdam, Netherlands*
[5]*Département de physique, génie physique et optique, CRAQ, Université Laval, Québec, Canada G1K 7P4*
[6]*GEPI, Observatoire de Paris, CNRS, Université Paris Diderot, 5 place Jules Janssen, 92190 Meudon, France*
[7]*Royal Observatory of Belgium, 3 avenue circulaire, 1180 Brussels, Belgium*
[8]*Shelyak Instruments, Les Roussets, 38420 Revel, France*

Accepted 2009 June 8. Received 2009 May 22; in original form 2008 December 21

ABSTRACT

We have obtained 40 high-resolution circular spectropolarimetric measurements of 12 slowly pulsating B (SPB) stars, eight β Cephei stars and two Be stars with the Echelle Spectropolarimetric Device for the Observation of Stars at CFHT (ESPaDOnS) and Narval spectropolarimeters. The aim of these observations is to evaluate recent claims of a high incidence of magnetic field detections in stars of these types obtained using low-resolution spectropolarimetry by Hubrig et al. The precision achieved is generally comparable to or superior to that obtained by Hubrig et al., although our new observations are distinguished by their resolution of metallic and He line profiles, and their consequent sensitivity to magnetic fields of zero net longitudinal component. In the SPB stars, we confirm the detection of magnetic field in one star (16 Peg), but find no evidence of the presence of fields in the remaining 11. In the β Cep stars, we detect a field in ξ^1 CMa, but not in any of the remaining seven stars. Finally, neither of the two B-type emission-line stars shows any evidence of magnetic field. Based on our results, we conclude that fields are not common in SPB, β Cep and B-type emission-line stars, consistent with the general rarity of fields in the broader population of main sequence B-type stars. A relatively small, systematic underestimation of the error bars associated with the UV Focal Reducer and Low Dispersion Spectrograph for the Very Large Telescope (FORS1) longitudinal field measurements of Hubrig et al. could in large part explain the discrepancy between their results and those presented here.

Key words: stars: magnetic fields – stars: pulsations.

1 INTRODUCTION

Some B-type stars have been established to host strong, organized magnetic fields (e.g. Bohlender et al. 1987, Bohlender, Landstreet & Thompson 1993). The first such stars discovered were main sequence helium-weak and helium-strong stars (Borra & Landstreet 1979, Borra, Landstreet & Thompson 1983) – objects which also display strong photospheric chemical abundance anomalies. The lack of similar anomalies in the spectra of the large majority of other B-type stars was taken as evidence that magnetic fields are relatively rare in such stars. It, therefore, came as a surprise when Henrichs et al. (2000) reported the detection of a 300 G dipolar magnetic field in the chemically normal, pulsating B1IV star β Cephei. This discovery was soon followed by reports of magnetic fields in the β Cep star V2052 Oph (Neiner et al. 2003c), the slowly pulsating B (SPB) star ζ Cas (Neiner et al. 2003a) and the classical Be star ω Ori (Neiner et al. 2003b). More recently, Donati et al. (2006) have reported a field in the bright B0.5V star τ Sco, and Petit et al. (2008) and Alecian et al. (2008a) have established the existence of fields in the very young early B-type stars HD 36982 and HD 37061 (in the ONC), NGC 6611-601 and NGC 2244-201.

The discovery of fields in this diverse population of B-type stars has generated significant interest in their magnetic properties, for several reasons. These stars exhibit a tremendous range of physical phenomena (pulsation, rapid rotation, mass loss, accretion and decretion discs, etc.) capable of highlighting the interaction of the magnetic field with the stellar plasma and their intense radiation

⋆E-mail: James.Silvester@rmc.ca

fields. Many also end their lives in Type II supernovae (Stankov & Handler 2005), and are progenitors of (strongly magnetic) neutron stars.

Recently, Hubrig et al. (2006, 2009) (hereafter referred to as H06 and H09, respectively) reported longitudinal magnetic field measurements of 61 pulsating or candidate pulsating B-type stars (45 SPB stars and 16 β Cep stars), acquired using the FORS1 spectropolarimeter at the European Southern Observatory (ESO) very large telescope (VLT). In this large sample, H09 claimed detection (with $>3\sigma$ confidence) of 21 magnetic fields in the 45 SPB stars, corresponding to 47 per cent of the SPB sample. They also reported the detection of fields in five of 16 β Cep stars. In addition, Hubrig et al. (2007), hereafter referred to as H07, performed a similar analysis of observations of 15 classical Be stars, reporting significant detections of fields in three of these targets. These results suggest that magnetic fields may be significantly more common in pulsating B-type stars and Be stars than was previously assumed, and possibly that all SPB stars host organized magnetic fields.

To verify these potentially very important results, we have undertaken high-resolution circular polarization spectroscopy of a sample of 22 SPB, β Cep and Be stars using the powerful ESPaDOnS and Narval high-resolution spectropolarimeters at the Canada–France–Hawaii Telescope (CFHT, on the Big Island of Hawaii) and the Télescope Bernard Lyot (TBL, at Pic du Midi Observatory in southern France).

2 TARGETS AND OBSERVATIONS

Targets for this study were selected primarily from those stars observed by H09, and to a lesser extent by H06 and H07, that were observable from the CFHT and/or from TBL. Three additional β Cep stars were also observed. Because many of the stars observed by H06, H07 and H09 are located in the southern hemisphere, only 19 of their targets could be observed from CFHT and Pic du Midi. The complete list of our 22 targets is provided in Table 1.

The selected sample of eight β Cep stars is shown in Table 1. H09 reported the detection of a 366 ± 11 G longitudinal magnetic field in ξ^1 CMa and a field of -49 ± 13 G in δ Cet. Four additional β Cep stars were undetected by those authors, with typical uncertainties of about 30 G. The three remaining β Cep stars HD 886, HD 207330 and HD 218376 were not observed by H06, H07 and H09.

The SPB stars are of particular interest, because H09 reported that nearly half of their SPB sample is magnetic. Of the 12 SPB stars in our sample (all of which were observed by H06 and H09), H06 and H09 claim detection of magnetic field in six. Finally, as part of this study, two B-type emission-line stars (υ Sgr[1] and χ Oph) were also observed. Both of the stars are considered by H07 to host weak magnetic fields.

To evaluate the presence of magnetic fields in our targets, we have acquired high-resolution circular polarization (Stokes V) spectroscopy of our targets. The observations reported here were obtained over a period of about a year, using the ESPaDOnS and Narval spectropolarimeters, the cross-dispersed echelle spectropolarimeters built for the CFHT and Bernard Lyot Telescope, respectively. These instruments are effectively identical, and are conceptually similar to the Multi Site Continuous Spectroscopy (MuSiCoS) spectropolarimeter which was used extensively for high-precision magnetic measurements (e.g. Wade et al. 2000a; Donati et al. 2001; Shorlin et al. 2002). ESPaDOnS and Narval are, however, characterized by a factor of about 20 times higher efficiency.

[1] Koubský et al. (2006) report that υ Sgr is in fact a mass-transfer binary in the initial phases of mass transfer, in which the emission-lines arise from the disc.

Table 1. Stars observed in this investigation. Included are effective temperature (as reported by H06, H07, H09) and projected rotational velocity obtained as described in Section 3.

Star	Other name	Spectral type	$T_{\rm eff}$ (K)	$v \sin i$ (km s^{-1})
		β Cephei stars		
HD 886	γ Peg	B2 IV	22 500	10 ± 5
HD 16582	δ Cet	B2 IV	23 000	8 ± 5
HD 29248	ν Eri	B2 III	23 000	34 ± 5
HD 44743	β CMa	B1 II-II	26 000	25 ± 5
HD 46328	ξ^1 Cma	B1 III	27 000	14 ± 5
HD 129929	V836 Cen	B2	24 000	25 ± 5
HD 207330	81 Cyg	B3 III	18 000	50 ± 5
HD 218376	1 Cas	B0.5 IV	27 000	25 ± 5
		Slowly pulsating B stars		
HD 3379	53 Psc	B2.5 IV	17 300	37 ± 10
HD 24587	33 Eri	B5 V, SB1	13 900	25 ± 5
HD 26326	GU Eri	B5 IV	15 000	19 ± 10
HD 28114	V1143 Tau	B6 IV	14 600	14 ± 5
HD 34798	YZ Lep	B5 IV-V	15 600	41 ± 10
HD 45284	BD-07 1424	B8, SB2	14 500	97 ± 10
HD 46005	V727 Mon	B8 V	21 000	150 ± 20
HD 138764	IU Lib	B6 IV	14 000	32 ± 5
HD 140873	PT Ser	B8 III, SB2	13 900	88 ± 10
HD 181558	V4199 Sgr	B5 III	14 700	25 ± 5
HD 206540	BD +10 4604	B5 IV	14 000	12 ± 5
HD 208057	16 Peg	B3 V, SB ?	16 700	145 ± 20
		B-type emission-line stars		
HD 148184	χ Oph	B2Vne	24 000	155 ± 20
HD 181615	υ Sgr	B2Vpe	23 000	33 ± 5

The polarization analyser is located at the Cassegrain focus of the telescope. Light passing through the pinhole aperture traverses a rotatable $\lambda/2$ waveplate, a fixed $\lambda/4$ waveplate, a second rotatable $\lambda/2$ waveplate, and finally a small-angle Wollaston prism, followed by a lens which refocuses the (now double) star image on the input of two optical fibres. This relatively complex polarization analyser, which employs Fresnel rhombs, allows for essentially achromatic analysis over the large bandpass (3700 Å to 1.04 μm).

The two output beams from the Wollaston prism, which have been analysed into the two components of circular polarization, are then carried by the pair of optical fibres to a stationary and temperature-controlled cross-dispersed spectrograph where two interleaved spectra are formed, covering virtually the entire desired wavelength range with a resolving power of $R \simeq 65\,000$. The I component of the stellar Stokes vector is formed by adding the two corresponding spectra, while the V polarization component is obtained essentially from the difference of the two spectra. To minimize systematic errors due to small misalignments, differences in transmission, effects of seeing, etc., one complete observation of a star consists of four successive spectra; for the second and third, the waveplate settings are changed so as to exchange the positions of the two analysed spectra on the CCD (c.f. Donati et al. 1997).

The actual reduction of observations is carried out at the observatories using the dedicated software package LIBRE-ESPRIT, which yields both the I spectrum and the V circular polarization spectrum of each star observed. Each reduced spectrum is normalized order-by-order using a FORTRAN code specifically optimized to fit the continuum of hot stars with emission lines.

Table 2. Log of observations and magnetic field measurements obtained with ESPaDOnS and Narval. The Julian Date of each observation is reported, along with the exposure time, peak S/N per 1.8 km s^{-1} pixel in the reduced spectrum, resultant S/N per 2.6 km s^{-1} LSD profile pixel and computed gain, integration limits for evaluation of the longitudinal magnetic field, Stokes *V* detection diagnosis (DD, definite detection; MD, marginal detection; ND, no detection) and probability, and the longitudinal field measurement obtained by evaluation of equation (1). Marginal and definite Stokes *V* detections, and longitudinal field measurements significant at greater than 3σ, are shown in bold. Also shown are the longitudinal fields reported by H06, H07 and H09.

HD	JD −2 400 000	Exp time (s)	Peak S/N	LSD S/N	LSD gain	Int Limits (km s^{-1})	Detection flag	Detection probability	B_ℓ (G)	H06, H07, H09 B_ℓ (G)
					β Cephei stars					
HD 886	54817.7174	80	967	10 235	10.6	−47/50	ND	0.001	6 ± 11	
HD 16582	54817.8043	280	1021	10 808	10.6	−45/55	ND	0.001	2 ± 10	$\mathbf{-49 \pm 13}$
HD 29248	54489.98272	200	503	4790	9.5	−34/130	ND	0.005	9 ± 38	-41 ± 28
HD 44743	54488.9702	60	1015	11 568	11.4	−34/100	ND	0.899	-31 ± 13	-44 ± 29
HD 46328	54488.98129	247	738	6230	8.4	−11/60	**DD**	1.000	$\mathbf{338 \pm 11}$	$\mathbf{330 \pm 45}$
HD 129929	54164.0772	1600	291	2886	9.9	−3/115	ND	0.026	-14 ± 35	-80 ± 35
HD 207330	54819.7901	320	757	8369	11.1	−91/65	ND	0.004	8 ± 24	
HD 218376	54815.7721	480	703	6678	9.5	−89/76	ND	0.001	13 ± 23	
					Slowly pulsating B stars					
HD 3379	54376.9734	600	660	10 546	16.0	−138/78	ND	0.127	-97 ± 77	$\mathbf{155 \pm 42}$
	54352.6918	2880	901	14 374	16.0	49/81	ND	0.194	-49 ± 53	
	54353.5664	2200	781	11 785	15.1	−115/76	ND	0.037	1 ± 40	
	54354.6115	2400	757	11 869	15.7	54/87	ND	0.012	-68 ± 77	
	54355.6268	2800	834	12 861	15.4	56/89	ND	0.005	81 ± 64	
	54356.6592	4520	877	13 555	15.5	−115/82	ND	0.346	46 ± 35	
HD 24587	54373.9702	300	745	12 553	16.8	−19/79	ND	0.154	-48 ± 34	$\mathbf{-353 \pm 82}$
HD 26326	54374.9800	600	588	12 454	21.2	−34/63	ND	0.066	-18 ± 22	-30 ± 33
HD 28114	54373.9793	600	531	6831	12.9	−27/50	ND	0.632	-28 ± 30	$\mathbf{107 \pm 33}$
HD 34798	54375.9794	700	700	7529	10.8	−40/71	ND	0.377	-10 ± 35	-99 ± 45
HD 45284	54488.9926	1120	374	6192	16.6	−63/100	ND	0.642	-1 ± 89	-55 ± 50
HD 46005	54489.9998	1600	380	5004	13.2	121/154	ND	0.676	6 ± 203	2 ± 79
HD 138764	54168.0624	600	897	15 056	16.8	−47/42	ND	0.048	-2 ± 14	146 ± 57
HD 140873	54168.0728	600	820	13 978	17.0	−89/86	ND	0.440	14 ± 29	$\mathbf{99 \pm 31}$
	54111.7501	2400	611	10 203	16.7	−102/76	ND	0.024	32 ± 67	
	54111.7723	2400	651	11 039	17.0	−102/79	ND	0.052	-35 ± 63	
	54114.7410	1680	697	8725	12.5	−109/65	ND	0.010	19 ± 74	
	54116.7550	1680	402	5866	14.6	−107/65	ND	0.114	60 ± 46	
	54277.3901	1680	764	12 898	16.9	−86/81	ND	0.140	26 ± 50	
	54277.4119	1680	719	14 012	19.5	−86/81	ND	0.001	15 ± 44	
	54278.3945	1680	831	12 985	15.6	−81/92	ND	0.085	-19 ± 50	
HD 181558	54293.5141	2400	603	10 111	16.8	−73/11	ND	0.111	-25 ± 21	$\mathbf{-104 \pm 32}$
	54293.5442	2400	554	9324	16.8	−71/11	ND	0.299	-13 ± 22	
HD 206540	54374.9051	600	524	8751	16.7	−34/29	ND	0.041	-13 ± 18	-2 ± 27
HD 208057	54371.9016	600	1092	17 295	15.8	−160/107	**MD**	0.998	-47 ± 50	$\mathbf{-156 \pm 31}$
					B-type emission-line stars					
HD 148184	54635.4480	3600	1770	21 815	12.3	204/258	ND	0.077	-73 ± 63	$\mathbf{136 \pm 16}$
	54636.4437	3600	1435	18 051	12.6	217/245	ND	0.421	13 ± 75	
	54637.4400	3600		15 025		217/245	ND	0.617	-96 ± 112	
	54638.4821	3600	1017	12 637	12.4	207/234	ND	0.021	43 ± 72	
HD 181615	54635.5881	3600	1786	22 815	12.7	−55/45	ND	0.798	16 ± 7	$\mathbf{38 \pm 10}$
	54636.5875	3600	1594	20 298	12.7	−52/47	ND	0.005	-6 ± 8	
	54638.6214	3600	1071	13 386	12.5	−47/52	ND	0.201	-15 ± 12	

A diagnostic null spectrum called the *N* spectrum, computed by combining the four observations of polarization in such a way as to have real polarization cancel out, is also calculated by LIBRE-ESPRIT. The *N* spectrum tests the system for spurious polarization signals. In all of our observations, the *N* spectrum is quite featureless, as expected. The final spectra consist of ASCII files tabulating I, V, N, and the estimated uncertainty per pixel as a function of wavelength, order by order.

In this study, 40 spectra of the 22 B-type targets were acquired. The peak signal-to-noise ratios (S/N) of the reduced one-dimensional spectra range from 300 to 1700 per 1.8 km s^{-1} spectral pixel. The log of observations is reported in Table 2.

3 ANALYSIS

The spectra were analysed using the least-squares deconvolution (LSD) multiline analysis method (Donati et al. 1997). LSD produces mean Stokes *I* and *V* profiles using essentially all metallic and He lines in the stellar spectrum, assuming that the observed spectrum can be represented as the convolution of a single 'mean' line profile with an underlying spectrum of unbroadened metal and helium lines of appropriate wavelength, depth and Landé factor (the 'line mask' computed using spectrum synthesis; cf. Wade et al. 2000a). The LSD model allows the computation of single, average Stokes *I* and *V* line profiles, representative of essentially all lines in the stellar

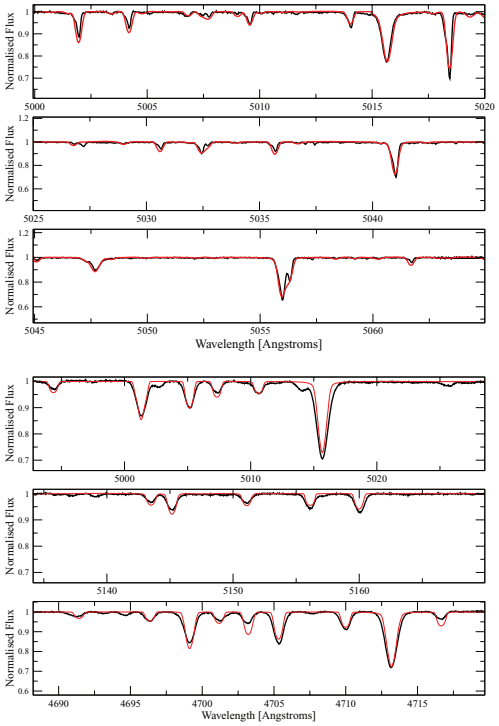

Figure 1. Top frame: comparison between a solar abundance model spectrum (smooth red curve) for a temperature of 14 000 K and the observation of HD 206540 (black crosses). Lower frame: comparison between a solar abundance model spectrum (smooth red curve) for a temperature of 27 000 K and the observation of HD 44743 (black crosses). The synthetic models acceptably reproduce the spectrum. This supports the use of solar abundance line masks in the LSD extraction.

spectrum, usually characterized by a S/N dramatically higher than that of individual spectral lines. Line masks for this study were compiled using Vienna Atomic Line Data base (VALD; Kupka et al. 1999) 'extract stellar' requests, with effective temperature and surface gravity appropriate to each target, and assuming solar abundances. As discussed by Shorlin et al. (2002), the LSD S/N is only weakly sensitive to the line-depth cut-off employed to populate the mask. Following their results, we have chosen to employ a line-depth cut-off equal to 10 per cent of the continuum. Imposing such a cut-off has a related advantage: because weaker lines are less likely to have published experimental Landé factors (and to generally have more poorly determined atomic data), we pre-filter our line list to (statistically) exclude those lines with the poorest data. Except for the line-depth cut-off, elimination of Balmer lines and restriction of the mask to the ESPaDOnS/Narval spectral range, no other line selection has generally been performed.

To verify the suitability of these masks, synthetic spectra corresponding to the mask parameters and content were computed and compared to the observations. For SPB and β Cep stars, an acceptable agreement was always obtained. For Be stars, an additional filtering of the mask was performed to exclude lines identified in the observations as being significantly affected by circumstellar emission. The agreement between a solar abundance synthetic spectrum and the observation of SPB star HD 206540 and the β Cep star HD 44743 for a small wavelength window is illustrated in Fig. 1. For a typical SPB star ($T_{\rm eff} = 14\,000$ K), 520 lines were included in the mask. For a typical β Cep star ($T_{\rm eff} = 25\,000$ K), 260 were included. For the two B-type emission-line stars, the filtered mask contained 177 lines. Although the number of strong lines, as well as the total number of lines, decreases with increasing temperature, the fraction of lines between a depth of 0.1 and 0.3 is around 80 per cent for all line masks used.

The LSD procedure propagates the formal error bars associated with each spectral pixel through the deconvolution. Because the computed LSD spectrum (the convolution of the deconvolved mean profile with the line mask) represents a highly simplified model of the spectrum, the overall agreement between the model and observations is generally relatively poor. To bring the observed and model spectrum into formal agreement, we interpret their mutual differences as random noise and scale the error bars associated with each pixel in the LSD profile in order to yield a final reduced χ^2 of the model relative to the observations that is equal to unity (Wade et al. 2000a). This has the effect of assigning errors to the LSD profile that are reflective of the real uncertainties of the modelling. When a magnetic field is present, each spectral line produces an associated Stokes V signature, resulting in a relatively complex Stokes V spectrum. Because the LSD model is unable to reproduce the details of this spectrum, the discrepancies are relatively severe, significant scaling of the error bars is required, and the uncertainties are dominated by the limitations of the model. On the other hand, when no magnetic field is present, the Stokes V spectrum is featureless. The model is able to fit the Stokes V spectrum essentially within the formal errors, relatively little scaling is required, and the uncertainties are dominated by photon noise. The procedures used to derive the uncertainties have been extensively tested, and shown to generate assigned uncertainties which are consistent with the real scatter of observations for both magnetic and non-magnetic standards (e.g. Wade et al. 2000a; Shorlin et al. 2002; Chadid et al. 2004; Alecian et al. 2008b). The LSD profiles computed from the new spectra, one for each of the sample stars, are presented in Figs 2 and 3.

The presence or absence of a magnetic field detection was evaluated using two methods. First, we used the statistical test described by Donati, Semel & Rees (1992) and Donati et al. (1997) to diagnose the presence of a signal in the LSD V and N profiles. In this method, a signal is 'definitely' detected if the associated detection probability of Stokes V within the spectral line is larger than 99.999 per cent (corresponding to a false alarm probability smaller than 10^{-5}), and if the detection probabilities both outside the line and in the diagnostic null within the line are insignificant. A 'marginal' detection corresponds to a detection probability between 99.9 and 99.999 per cent (false alarm probability between 10^{-3} and 10^{-5}). A detection probability below 99.9 per cent corresponds to no formal detection.

The second method involved inferring the mean longitudinal magnetic field, evaluated by computing the first-order moment of the Stokes V profile within the line according to

$$B_\ell = -2.14 \times 10^{11} \frac{\int v V(v)\,{\rm d}v}{\lambda g c \int [1 - I(v)]\,{\rm d}v} \qquad (1)$$

(Mathys 1989; Wade et al. 2000a), where g is the mean Landé factor and λ is the mean wavelength of all the lines included in the mask. LSD profiles were locally renormalized to a continuum level of 1.0 before evaluation of equation (1). Uncertainties associated with B_ℓ were computed by propagating the formal uncertainties of each LSD spectral pixel through equation (1).

The integration range (in km s^{-1}) associated with equation (1) was computed individually for each LSD profile. First, we identified the first and last point in the Stokes I profile for which the flux was equal to 85 per cent of the continuum. To correct for

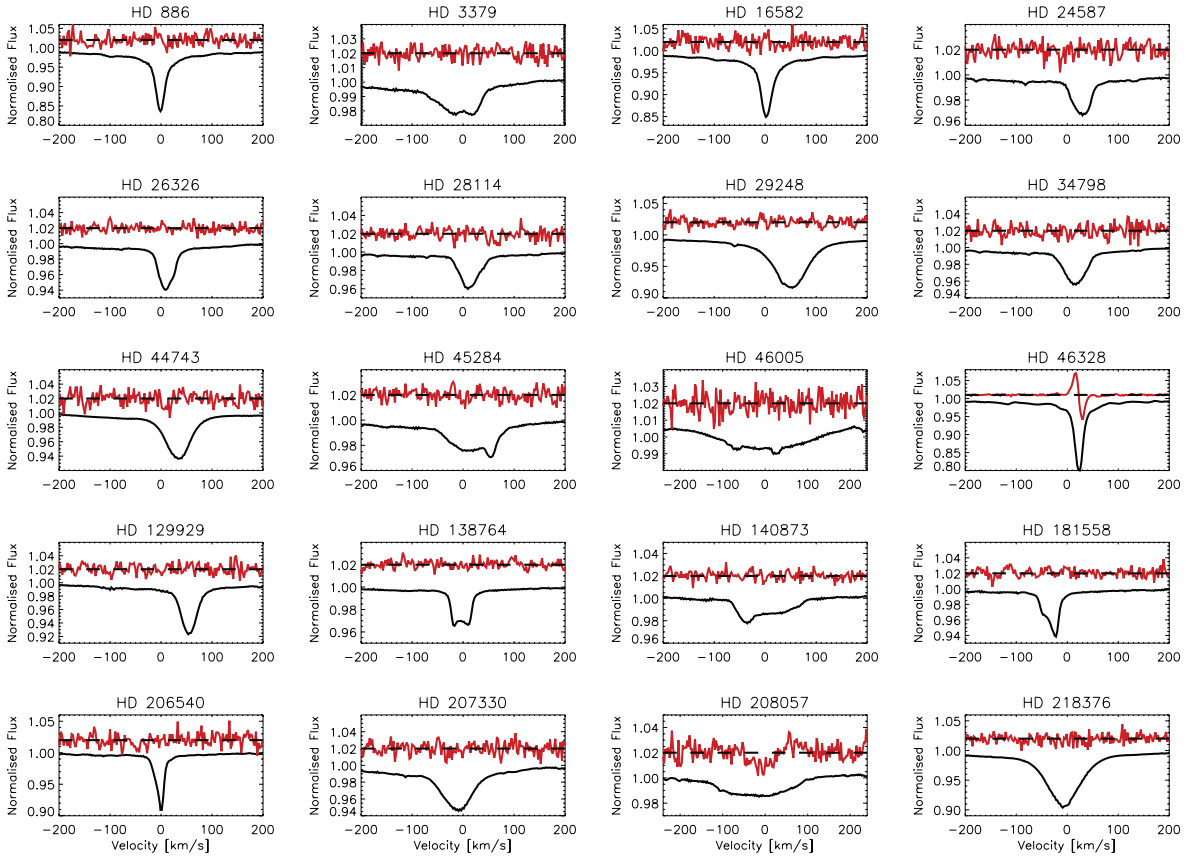

Figure 2. Least-squares deconvolved profiles of the SPB and β Cep stars (for stars with multiple observations, a single example is shown). Each panel represents a different star, with the bottom curve showing the LSD mean intensity (Stokes *I*) profile and the top curve showing the circular polarization Stokes *V* profile. Note the frequently asymmetric or otherwise distorted profile shapes due to pulsation and binarity.

errors due to line profile structure (e.g. binarity), these preliminary integration ranges were then visually inspected and adjusted to best match the observed profile span. The integration ranges employed for each profile are reported in Table 2. While this procedure can result in integration ranges of different LSD profiles of the same star differing significantly (e.g. variable SB2 HD 140873 in Table 2), this careful adjustment of the integration range allows us to optimize the magnetic diagnosis to the detailed shape of the line profile. This, therefore, represents an important strength of this technique – one that is not possible at the low resolution of FORS1.

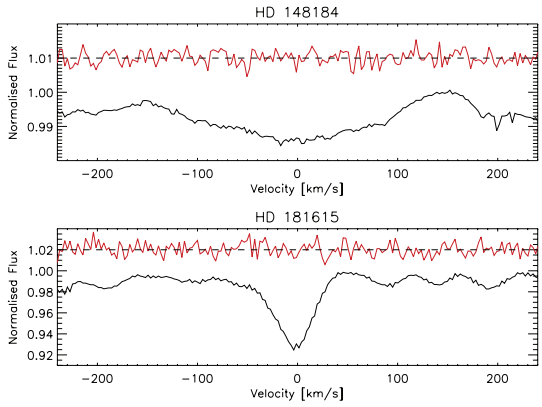

Figure 3. Representative least-squares deconvolved profiles of the two B-type emission-line stars. Each panel represents a different star, with the bottom curve showing the LSD mean intensity (Stokes *I*) profile and the top curve showing the circular polarization Stokes *V* profile. Note the relatively poor quality of the deconvolution (distortion of the continuum, for example, due to the smaller number of lines in the mask) as compared to the profiles shown in Fig. 2.

It is important to note that the longitudinal field is used only as a statistical indicator of the field strength and not as the primary diagnostic of the presence of a magnetic field. This is because a large variety of magnetic configurations can produce a mean longitudinal field component that is formally null (i.e. for which the first-order moment of Stokes *V* is zero – a profile approximately symmetric about the centre-of-gravity of the line). However, nearly all of these configurations will generate a detectable Stokes *V* signature in the velocity-resolved line profile. As a consequence, high-resolution spectropolarimetry combined with LSD has been repeatedly shown to be effective at detecting relatively complex magnetic configurations, in both hot (e.g. Donati et al. 2006) and cool (e.g. Donati et al. 1999) stars.

In addition to measuring the longitudinal magnetic field from each LSD profile, we also inferred projected rotational velocities using the automated fitting procedure included in the BinMag IDL visualization tool (constructed by O. Kochukhov). This procedure compares individual observed line profiles with synthesized profiles computed for appropriate temperature and gravity. Multiple metallic lines were fit in each spectrum to achieve a distribution of $v \sin i$ measurements. The resulting means and deviations are reported in Table 1. The derived uncertainties are relatively high due to the distortion of line profiles by pulsation and binarity. The majority of the derived $v \sin i$s are in good agreement with those

reported by H06, although our adopted uncertainties are somewhat larger.

Our measured detection probabilities and longitudinal fields, as well as the FORS1 longitudinal fields reported by H06, H07 and H09, are reported in Table 2.

4 RESULTS

In our sample of 22 B-type stars, we obtain one definite detection, one marginal detection and 20 non-detections of Stokes V signatures reflecting the presence of photospheric magnetic fields. Among the β Cep stars, we obtain a clear detection of magnetic field in ξ^1 CMa, which shows strong Stokes V signatures in the LSD profile (Fig. 2), as well as in individual spectral lines (Fig. 4). The longitudinal magnetic field measured from our single spectrum of this star is 338 $\pm$ 11 G, formally consistent with the measurement by H06 and H09. No fields are detected in the remaining 7 β Cep stars, with typical longitudinal field formal errors of a few tens of G. In contrast, H09 report the β Cep star δ Cet to be magnetic ($B_\ell = -49 \pm 13$ G), a result that we do not confirm ($B_\ell = 2 \pm 10$ G).

Among the SPB stars, we obtain a marginal detection of a Stokes V signature in the LSD profile of 16 Peg. Additional Narval observations of this star (Henrichs et al. 2009) confirm the detection of the field, and provide constraints on the field geometry and the stellar rotational period. None of the remaining SPB targets shows any evidence of magnetic field, with a median longitudinal field error bar of 45 G. Of SPB stars which were not detected by us, H09 claim detections of 5: HD 3379, HD 24587, HD 28114, HD 140873 and HD 181588. We find no evidence of fields in these stars, with error bars comparable to those of H06 and H09. Moreover, for three of these stars we have obtained multiple null results. Given the high quality of the spectra and the sensitivity of high-resolution spectropolarimetry to the magnetic field at essentially all rotational phases, we conclude that it is highly likely that none of these five SPB stars is in fact magnetic.

Finally, in the two B-type emission-line stars observed in this study (HD 148184 and HD 181615) no magnetic fields are detected. Multiple observations were acquired for both stars. Longitudinal field error bars smaller than 10 G were achieved for HD 181615, allowing us to conclude confidently that no field is present. However, the error bars for the broader-lined star HD 148184 are rather larger, and while we find no evidence of a field at the $\sim$150 G level as reported by H07, such a field could in principle remain undetected in our observations.

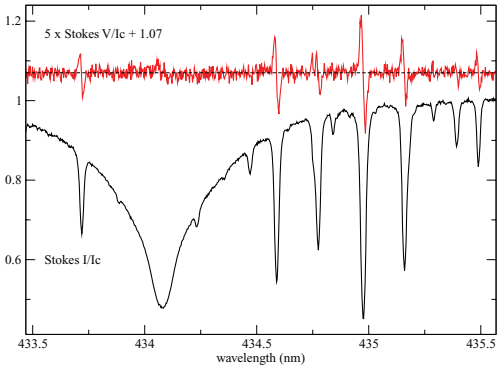

Figure 4. Stokes V signatures in individual lines in the spectrum of ξ^1 CMa in the region of Hγ.

5 DISCUSSION AND CONCLUSIONS

The basic results of this study are the confirmation of magnetic fields in the β Cep star ξ^1 CMa (HD 46328) and the SPB star 16 Peg (HD 208057), and the failure to detect fields in 20 other β Cep, SPB and Be stars, eight of which were claimed to be magnetic by H06, H07 and H09. The β Cep star ξ^1 CMa has relatively sharp lines ($v \sin i = 14$ km s^{-1}), and we infer a strong magnetic field ($B_\ell = 338 \pm 11$ G) which is consistent with that reported by H09. The SPB star 16 Peg is a relatively rapid rotator, with $v \sin i = 145$ km s^{-1}. We measure a weak longitudinal magnetic field of 47 $\pm$ 50 G.[2] Henrichs et al. (2009) have obtained many Narval Stokes V spectra of this star in which the Stokes V signature was detected repeatedly. Those authors inferred an organized surface magnetic field with longitudinal field extrema of $\approx \pm 140$ G.

For the other eight stars reported to be magnetic by H06, H07 and H09, we are unable to confirm their detections. While the generation of spurious field *detections* due to instrumental and astrophysical effects is a real danger in stellar magnetometry, it is very difficult to engineer scenarios that produce spurious *non-detections* of Stokes V signatures, particularly in a systematic manner for a large sample of stars. It, therefore, seems very unlikely that the null results obtained here for many stars are a result of a systematic inability to detect magnetic fields. This is supported by our detection of magnetic fields in 16 Peg and ξ^1 CMa (notwithstanding the fact that the longitudinal field of 16 Peg is formally null). That our error bars are not overestimated is supported by the reduced χ^2 of the longitudinal fields we measure (see e.g. Bohlender et al. 1993). For the non-detections, the longitudinal field reduced χ^2 is 0.96, indicating that the longitudinal field error bars are fully consistent with the scatter of the measurements. In addition, the distribution of longitudinal fields measured from the diagnostic N profiles (which should correspond to zero magnetic field) are statistically consistent with the expected normal distribution about a mean of zero, with a dispersion in agreement with the inferred Stokes V error bars.

The Stokes V signature amplitude will vary due to stellar rotation: could it be that we have observed these stars when the signature is weak and undetectable? While possible, this is statistically unlikely. First, if we take the results of H06, H07 and H09 at face value, then the magnetic strengths and geometries of these stars must favour magnetic detection (because so many were detected by them). Secondly, it can be easily confirmed by inspecting the Stokes V profile phase variations of real magnetic stars (e.g. Wade et al. 2000b) that the signature amplitude remains relatively constant as a function of stellar rotation. Both of these facts suggest that our failure to detect magnetic fields in these stars is unrelated to phase or geometry effects.

An examination of Fig. 2 reveals that many of the LSD profiles show asymmetries and distortions (HD 3379, HD 45284, HD 46005, HD 138764, HD 140873, HD 181558, HD 208056). Could it be that these properties impair our ability to detect Stokes V signatures? The peculiar line profile shapes likely result from a variety of processes, in particular binarity and pulsation. For example, both HD 45284 and HD 140873 are both confirmed SB2s. The other stars showing significant profile asymmetries may well also be spectroscopic binaries. However, the presence of the line profile of a companion to a magnetic star will not reduce or otherwise modify the Stokes V signature observed in high-resolution

[2] Recall that although the longitudinal field is not significantly detected, circular polarization is unambiguously detected in the LSD profile.

spectropolarimetry. Therefore, although the inferred longitudinal field and its uncertainty maybe modified somewhat (because we infer the field by integration over the entire composite profile), our ability to *detect* fields is not substantially affected.

Naturally, as this study focuses on pulsating stars, many of the observed profiles are distorted by pulsation. HD 138764 and 181558 appear to represent extreme examples of this phenomenon. While pulsation velocity fields will distort Stokes *V* profiles in a manner analogous to Stokes *I* (see Donati et al. 2001 for a nice illustration of this effect), there is no evidence to suggest that the Stokes *V* profiles are significantly more difficult to detect. In fact, the rapid temporal changes in line profile shapes due to pulsation are more likely to introduce spurious Stokes *V detections* (Schnerr et al. 2006), rather than to cause Stokes *V* signatures to disappear. It is also important to appreciate that the effects of pulsation and binarity, while discussed here in the context of high-resolution spectropolarimetry, are equally significant for low-resolution spectropolarimetry. The major difference is that the high-resolution spectra provide us with the capability to see and diagnose these effects, whereas they are essentially invisible in low-resolution spectra.

In conclusion, the present study confirms fields in only two stars of the H06, H07 and H09 sample: ξ^1 CMa and 16 Peg. We do not confirm the remaining detections. This inability to confirm the reported detections made using FORS1 poses a real problem, and clearly illustrates the need for further investigation. To underscore this need, we point out that of the 10 stars in our sample reported to be magnetic by H06, H07 and H09, just three are claimed by them to be detected at more than 4.5σ confidence – and we have confirmed fields in two of those. None of the remaining stars is detected by them at high significance. In fact, if their error bars were underestimated by just one-third ($\sim$33 per cent, the difference between $\sigma =$ 30 and 40 G), most of those detections would be transformed into sub-3σ non-detections. To our knowledge, no detailed investigation of the accuracy of the FORS1 error bars derived by these authors has ever been performed (in particular error bars below a few tens of G).

Outside of the present study and those of H06, H07 and H09, there are only a few cases of confirmed magnetic fields in β Cephei and SPB stars (β Cep itself, Henrichs et al. 2000; V2052 Oph, Neiner et al. 2003a; ζ Cas, Neiner et al. 2003b), and no confirmed detections of magnetic fields in classical Be stars. Magnetic fields, therefore, appear to be relatively rare in these classes of stars. We, therefore, propose that the incidence of fields with strengths detectable with current spectropolarimeters in these classes of stars merely reflects the (apparently rather low) incidence of fields in the larger population of stars at these spectral types, and is fundamentally unrelated to the physical properties that define these particular classes of stars.

ACKNOWLEDGMENTS

GAW acknowledges Discovery Grant support from the Natural Sciences and Engineering Research Council of Canada.

REFERENCES

Alecian E. et al., 2008a, A&A, 481, L99
Alecian E. et al., 2008b, MNRAS, 385, 391
Bohlender D. A., Landstreet J. D., Brown D. N., Thompson I. B., 1987, ApJ, 323, 325
Bohlender D. A., Landstreet J. D., Thompson I. B., 1993, A&A, 269, 355
Borra E. F., Landstreet J. D., 1979, ApJ, 228, 809
Borra E. F., Landstreet J. D., Thompson I., 1983, ApJS, 53, 151
Chadid M., Wade G. A., Shorlin S. L. S., Landstreet J. D., 2004, A&A, 413, 1087
Donati J.-F., Semel M., Rees D. E., 1992, A&A, 265, 669
Donati J.-F., Semel M., Carter B. D., Rees D. E., Collier Cameron A., 1997, MNRAS, 291, 658
Donati J.-F., Catala C., Wade G. A., Gallou G., Delaigue G., Rabou P., 1999, A&AS, 134, 149
Donati J.-F., Wade G. A., Babel J., Henrichs H. F., de Jong J. A., Harries T. J., 2001, MNRAS, 326, 1265
Donati J.-F., Howarth I. D., Bouret J.-C., Petit P., Catala C., Landstreet J., 2006, MNRAS, 365, L6
Henrichs H. F. et al., 2000, in Smith M. A., Henrichs H. F., Fabregat J., eds, ASP Conf. Ser. Vol. 214, IAU Colloq. 175, The Be Phenomenon in Early-Type Stars The Magnetic Field of β Cep and the Be Phenomenon. Astron. Soc. Pac., San Francisco, p. 324
Henrichs H. F. et al., 2009, in Strassmeier K. G., Kosovichev A. G., Beckman J. E., eds, IAU Symp. 259, Cosmic Magnetic Fields: From Planets, to Stars and Galaxies. Cambridge Univ. Press, Cambridge, p. 393
Hubrig S., Briquet M., Schöller M., De Cat P., Mathys G., Aerts C., 2006, MNRAS, 369, L61 (H06)
Hubrig S., Yudin R. V., Pogodin M., Schöller M., Peters G. J., 2007, Astron. Nachr., 328, 1133 (H07)
Hubrig S., Briquet M., De Cat P., Schöller M., Morel T., Ilyin I., 2009, Astron. Nachr., 330, 317 (H09)
Koubský P., Harmanec P., Yang S., Netolický M., Škoda P., Šlechta M., Korčáková D., 2006, A&A, 459, 849
Kupka F., Piskunov N., Ryabchikova T. A., Stempels H. C., Weiss W. W., 1999, A&AS, 138, 119
Mathys G., 1989, Fundam. Cosm. Phys., 13, 143
Neiner C., Geers V. C., Henrichs H. F., Floquet M., Frémat Y., Hubert A.-M., Preuss O., Wiersema K., 2003a, A&A, 406, 1019
Neiner C., Hubert A.-M., Frémat Y., Floquet M., Jankov S., Preuss O., Henrichs H. F., Zorec J., 2003b, A&A, 409, 275
Neiner C. et al., 2003c, A&A, 411, 565
Petit V., Wade G. A., Drissen L., Montmerle T., Alecian E., 2008, MNRAS, 387, L23
Schnerr R. S., Verdugo E., Henrichs H. F., Neiner C., 2006, A&A, 452, 969
Shorlin S. L. S., Wade G. A., Donati J.-F., Landstreet J. D., Petit P., Sigut T. A. A., Strasser S., 2002, A&A, 392, 637
Stankov A., Handler G., 2005, ApJS, 158, 193
Wade G. A., Donati J.-F., Landstreet J. D., Shorlin S. L. S., 2000a, MNRAS, 313, 851
Wade G. A., Donati J.-F., Landstreet J. D., Shorlin S. L. S., 2000b, MNRAS, 313, 823

This paper has been typeset from a TEX/LATEX file prepared by the author.